Chapter 2

Ground State Equilibrium Thermodynamics and Switching Kinetics of Bistable [2]Rotaxane Switched in Solution, Polymer Gels, and Molecular Electronic Devices

2.1 Introduction

One of the goals (1-3) of the field of molecular electronics is to be able to control the properties of molecular-based solid-state devices through chemical design and synthesis. Such control has been demonstrated (4-15) for passive devices, the simplest of which are molecular tunnel junction resistors consisting of a molecular monolayer, often a functionalized alkane, sandwiched between two conductors. Several groups have shown that the tunnel current varies exponentially with chain length (10, 12), although they have also found that atomistic details (4, 5, 7, 8, 14), such as the packing of the chains, the molecular alignment within the monolayer, and the nature of the electrodes (6, 9, 13), are all important.

Molecular rectifiers, typically represented by an electron donor-bridge-acceptor molecule extended between two electrodes (16), represent a more sophisticated passive device. Demonstrations of molecular control over current rectification have required a substantial effort by a number of groups (16-32), and have only been achieved within the past few years. Details such as the nature of the

molecule/electrode interface, the donor and acceptor molecular orbital energies, and the structure of the molecule within the device – i.e., the extension of the donor-bridge-acceptor between the two electrodes – are all important since rectification can arise from many areas within a junction (16-32).

Active molecular electronic (33) devices (switches) represent a significant jump in terms of molecular complexity. My research group has used electrochemically switchable, donor-acceptor, bistable [2]catenane and [2]rotaxane molecules within molecular switch tunnel junctions (MSTJs) (34-36). As in the case of the molecular tunnel junction resistors and rectifiers, MSTJs also represent a highly coupled molecule/electrode system (6, 9, 13, 37, 38). However, for the bistable [2]catenane and [2]rotaxane switches, there are a number of experimental parameters that can be measured to correlate molecular structure and solution-phase switching behavior with molecular electronic device switching properties. These parameters include colorimetric changes (39), shifts in electrochemical potentials (40, 41), and temperature dependent kinetics (39-41) for the cycling of the switch.

As an example, consider the redox-switchable [2]rotaxane **RATTF**$^{4+}$ illustrated in figure 2-1a. This bistable [2]rotaxane is composed of electron-accepting cyclobis(paraquat-*p*-phenylene) (CBPQT^{4+}) ring (blue) that encircles either a tetrathiafulvalene (TTF) unit (green) or a 1,5-dioxynapthalene (DNP) unit (red), both

electron-donating systems. This mechanically-interlocked molecular compound and other closely related bistable rotaxanes (10, 40, 42-47) as well as rotaxanes constructed from different donor-acceptor units (48-50) and from hydrogen-bonded systems (51-54) and transition metal templates (55-58), have been investigated in depth previously.
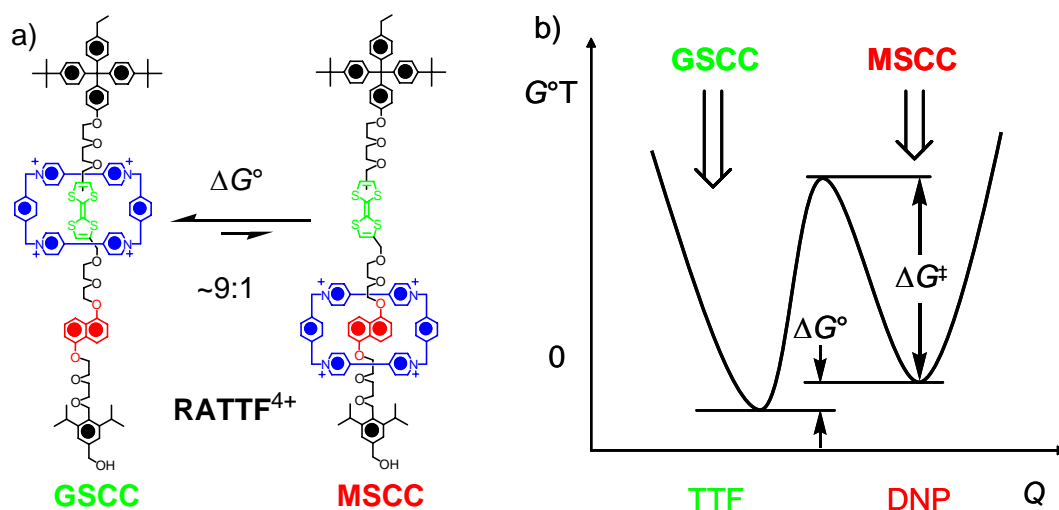
Figure 2-1. Molecular structure and potential energy surface of bistable [2]rotaxane. (a) Structural formulas of the two translational isomers of the bistable rotaxane **RATTF**$^{4+}$ corresponding to the ground state co-conformation (GSCC) and the metastable state co-conformation (MSCC). (b) Potential energy surface for the bistable **RATTF**$^{4+}$ where the energy wells correspond to the GSCC and MSCC. The free energy difference $\Delta G°$, between the wells and the free energy barrier to relaxation, $\Delta G^{\ddagger}$, from the MSCC to the GSCC are defined against a normal coordinate, Q, representing translation of the ring along the dumbbell component of the [2]rotaxane.

Under ambient conditions in acetonitrile solution, the $CBPQT^{4+}$ ring in **RATTF**$^{4+}$

encircles the TTF unit preferentially (>90%) with respect to the DNP unit. This

equilibrium is described by the $\Delta G°_{298}$ change shown in figure 2-1b where $\Delta G° =$

+1.6 kcal/mol when the $CBPQT^{4+}$ ring moves from the TTF to the DNP unit. Hence,

the co-conformation (CC) with the $CBPQT^{4+}$ ring encircling the TTF is unit is

referred to as the ground state co-conformation (GSCC). The first two oxidation states

of **RATTF**$^{4+}$ correspond to the $TTF^0 \rightarrow TTF^{•+} \rightarrow TTF^{2+}$ processes. Upon formation of

$TTF^{•+}$ cation radical, the Coulombic repulsion between the $CBPQT^{4+}$ ring and the

$TTF^{•+}$ results in translation of the ring to the DNP unit. This process is fast and is

believed to convert all of the GSCC into the MSCC. Although the Coulombic-driven

switching movement of the $CBPQT^{4+}$ ring has not been measured, I estimate that the

barrier corresponding to the mono- and di-cation $TTF^{2+/+}$ would be at least ~3 and ~6

kcal/mol less than the 16 kcal/mol barrier observed for the free energy barrier between

the MSCC and GSCC leading to room temperature time constants of $t \sim 500$ and 3 ms,

respectively. By the same reasoning, for the TTF^{2+} dication, the movement of the

$CBPQT^{4+}$ ring to results. When the $TTF^{•+}$ cation radical is reduced back to TTF^0, the

$CBPQT^{4+}$ ring remains around the DNP unit for a period of time. This translational

isomer of the GSCC is the metastable state co-conformation (MSCC). Recovery of

the MSCC/GSCC equilibrium distribution (~1:9) is an activated process.

This switching cycle can be detected by a number of experimental observations. First, the lowest oxidation potential (corresponding to $TTF^0 \rightarrow TTF^{\bullet+}$) of the GSCC is +490 mV, while that for the MSCC is +310 mV. (All potentials referenced to an Ag/AgCl electrode.) Second, the colors of GSCC- and MSCC-dominated solutions are green and red, respectively. Thus, electrochemistry and spectroscopy can be employed to quantify the MSCC/GSCC ratio in such a bistable rotaxane at any given time. Third, the (activated) relaxation of an MSCC- back to a GSCC-dominated distribution is temperature dependent and so the kinetic parameters may be quantified through time- and temperature-dependent measurements. For example, the $\Delta G^{\ddagger}_{298}$ for this process in the case (40) of **RATTF**$^{4+}$ in the solution phase is 16.2 ($\pm$ 0.3) kcal/mol.

My research group has reported on the MSCC $\rightarrow$ GSCC relaxation kinetics for a number of bistable [2]catenanes and [2]rotaxanes in several different environments, including (i) in acetonitrile solution (40), (ii) in monolayers ([2]rotaxanes only) bonded to the surfaces of Au working electrodes (41), and (iii) in solid-state polymer electrolytes (39). In the case of the acetonitrile solution and the polymer electrolyte devices, My research group has demonstrated (39, 40) that the relaxation kinetics were sensitive to both molecular structure and physical environment, although the overall switching mechanism remains the same. I extended these measurements to

include MSTJ devices, as well as establishing the ground-state equilibrium thermodynamics. Three bistable [2]rotaxanes – namely **RATTF**[4+], **RTTF**[4+] and **RBPTTF**[4+] – plus the control (59) [2]rotaxane **RBLOCK**[4+] were investigated.
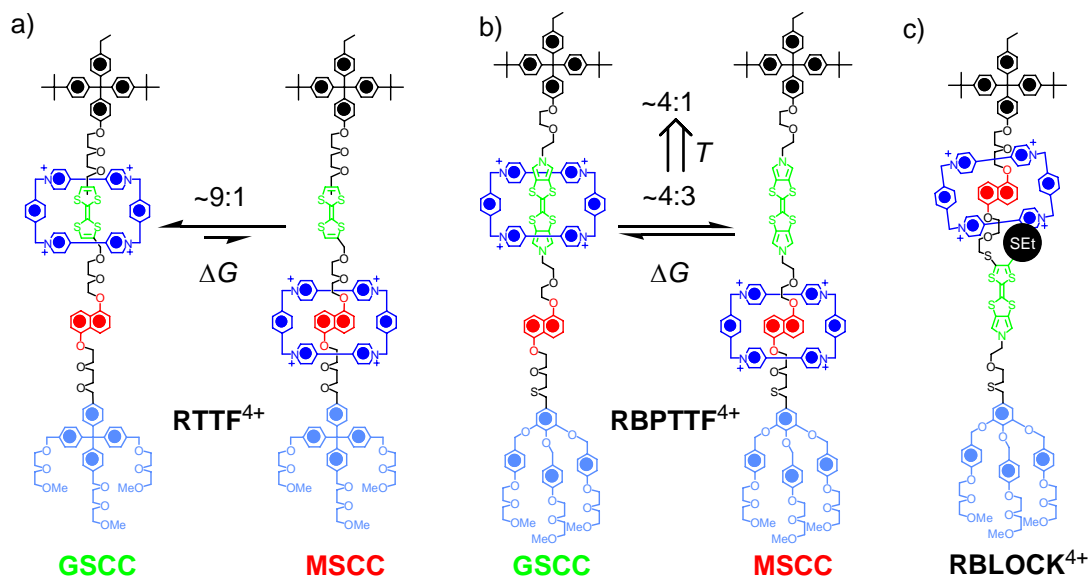
Figure 2-2. Structural formulas of the translational isomers of the bistable rotaxanes (a) **RTTF**[4+] and (b) **RBPTTF**[4+] both in their GSCC and MSCC. (c) Structural formula of the sterically-blocked (SEt) [2]rotaxane **RBLOCK**[4+] used in control studies.

It is evident from inspection of the structural formulas of these three [2]rotaxanes shown in figures 2-1 and 2-2 that **RATTF**[4+], **RTTF**[4+] and **RBPTTF**[4+] can exist at equilibrium as two translational isomers (or co-conformations). By contrast, **RBLOCK**[4+] has the CBPQT[4+] ring located exclusively around the DNP unit as a result of the presence of the bulky SEt group on the monopyrrolotetrathiafulvalene

unit acting as an effective steric barrier, thus preventing translational isomerism. The critical difference in the molecular structures between the **RATTF**[4+] and **RTTF**[4+] pair and the **RBPTTF**[4+] lies with the replacement of the simple TTF unit for the bispyrrolotetrathiafulvalene (BPTTF) unit (60). However, all three bistable rotaxanes have slightly different stoppers – **RATTF**[4+] bears a substituted benzylic alcohol function and both **RTTF**[4+] and **RBPTTF**[4+] have slightly different hydrophilic stoppers facilitating their incorporation into MSTJ devices. The major difference in the switching properties between these bistable rotaxanes is that the equilibrium MSCC/GSCC ratio (~1:9) for **RATTF**[4+] and **RTTF**[4+] is relatively temperature independent while the equilibrium MSCC/GSCC ratio (~1:4 at 298 K) for **RBPTTF**[4+] exhibits a strong temperature dependence. These thermodynamic differences will be rationalized in the following subchapter by reference to binding constants obtained by isothermal titration calorimetry (ITC) for the complexation of model guests containing TTF, BPTTF and DNP units, by the **CBPQT**[4+] host in acetonitrile solution at 298 K.

Previously my research group has hypothesized (34-37, 39, 40) that the GSCC corresponds to the low-conductance (switch-open) state of an MSTJ, while the MSCC corresponds to the high-conductance (switch-closed) state. This hypothesis is consistent with many observations, including the shift in the oxidation potential of the

TTF group that correlates with the switching from the GSCC to the MSCC structure.

In addition, Goddard's group (61, 62) has found by computational methods that the

MSCC structure has extended electron delocalization – and thus enhanced

conductivity – in comparison with the GSCC.

The switching kinetics of **RATTF**$^{4+}$, **RTTF**$^{4+}$ and **RBPTTF**$^{4+}$ should be

relatively similar. By contrast, the ground-state thermodynamics – and hence the

temperature-dependence of the switching amplitude – should be quite different. In this

study, I employed temperature dependent electrochemical and current-voltage

measurements to correlate *qualitatively* the thermodynamic properties of **RATTF**$^{4+}$ in

(i) acetonitrile solution, and (ii) solid-state polymer electrolytes, and of **RTTF**$^{4+}$ in

(iii) MSTJs together with **RBPTTF**$^{4+}$ across all three environments. I also correlated

quantitatively the MSCC $\rightarrow$ GSCC relaxation kinetics in these three different physical

environments. I find that the ground-state thermodynamic differences between the

pair of TTF-containing rotaxanes (**RATTF**$^{4+}$ and **RTTF**$^{4+}$) and **RBPTTF**$^{4+}$ are

relatively independent of physical environment, but strongly influenced by molecular

structure. I also find that, although the MSCC $\rightarrow$ GSCC relaxation kinetics exhibit a

strong environmental dependence in the case of all three rotaxanes, the switching

mechanism appears to be similar for all three compounds, and is robust and consistent

in all three environments. These findings allow me to refine our initial hypothesis

such that the high-conductance (switch-closed) state of an MSTJ still corresponds to the MSCC but that the low-conductance (switch-open) state is now related to the MSCC/GSCC ratio at equilibrium. These experiments provide a proof-of-principle for the control of molecular structure over a key device characteristic – temperature-dependent switching amplitudes in molecular electronic devices.

2.2 Molecular Design

Although the bistable [2]rotaxanes **RATTF**$^{4+}$, **RTTF**$^{4+}$ and **RBPTTF**$^{4+}$ all contain DNP sites, they differ in the first two contain a TTF unit and the third a BPTTF. In order to understand how these units influence the switching in these bistable rotaxanes, a series of model guests were investigated for their binding with the **CBPQT**$^{4+}$ host – as its tetrakis(hexafluorophosphate) salt – using ITC.

a)

TTF   **TTF-DEG**

BPTTF   **BPTTF-DEG**

DNP-OH   **DNP-DEG**

Guests

b)

Guest
+

K_a

CBPQT^{4+}
Host   Complex
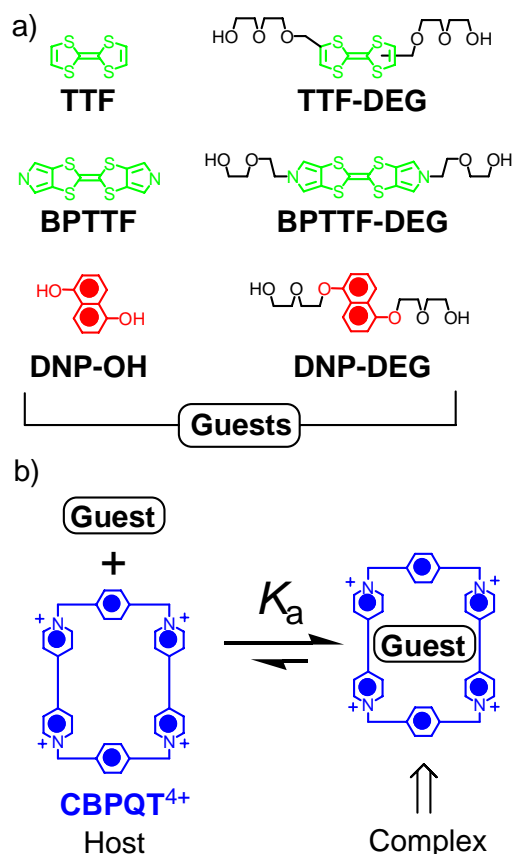
Figure 2-3. Control studies for designing stations in bistable [2]rotaxanes. (a) Structural formulas for a series of model guests. (b) Host-guest complexation between the **CBPQT**$^{4+}$ host and each of the guests.

The model guests are shown in figure 2-3a. They are tetrathiafulvalene (**TTF**) and its bispyrrolo derivative **BPTTF**; their diethyleneglycol-disubstituted derivatives **TTF-DEG** and **BPTTF-DEG**; and 1,5-dioxynaphthalene (**DNP-OH**) and its diethyleneglycol-disubstituted derivative **DNP-DEG**. Addition of the DEG substituents to the TTF and DNP units is known (63, 64) to enhance their binding constants with the **CBPQT**$^{4+}$ host to the extent that they increase by up to two orders

of magnitude. By contrast, the binding of **BPTTF** by the **CBPQT**[4+] host is already

quite high and only doubles.

Table 2-1. Thermodynamic binding data[a] corresponding to the complexation between **CBPQT**[4+] and the individual components of the bistable rotaxanes in MeCN determined by isothermal titration microcalorimetry at 298 K[38] in addition to solution-phase thermodynamic data of bistable rotaxanes.

Guest	$H°$ [b] (kcal/mol)	$S°$ [c] (cal/mol K)	$G°$ [d] (kcal/mol)	K_a [c] ($10^3 \, M^{-1}$)
TTF[e]	-10.64 ± 0.12	-18.1	-5.27 ± 0.03	6.9 ± 0.18
TTF-DEG	-14.21 ± 0.06	-22.1	-7.66 ± 0.07	380.0 ± 22.0
BPTTF[f]	-9.00 ± 0.02	-7.9	-6.66 ± 0.03	70.8 ± 0.98
BPTTF-DEG	-8.20 ± 1.70	-3.6	-7.17 ± 0.12	168.0 ± 17.0
DNP-OH[g]	-16.04 ± 8.11	-41.7	-3.63 ± 0.36	0.44 ± 0.13
DNP-DEG[h]	-15.41 ± 0.02	-30.8	-6.26 ± 0.04	36.4 ± 0.25
RATTF[4+] [i]	-2.82 ± 1.79[j]	-14.7 ± 6.8[j]	$+1.56 \pm 0.24$	
RBPTTF[4+] [j]	-6.64 ± 0.67	-26.0 ± 2.5	$+1.11 \pm 0.07$	

[a] A 0.39 mM standard solution of **CBPQT**[4+] was used for all titrations into which

solutions of various concentrations of guest were added in 5 μL aliquots (4.7 mM

TTF; 3.2 mM **TTF-DEG**; 5.0 mM **BPTTF**; 2.1 mM **BPTTF-DEG**; 5.4 mM **DNP-**

OH; 3.9 mM **DNP-DEG**). [b]Under the constant pressure of the instrument, $\Delta H°$ is

obtained from the heat of the reaction (65). [c]Fits were performed using software

provided by Microcal LLC software, and the stoichiometry of all complexes was

between 0.97 and 1.03 indicating a 1:1 complex was formed. [d] Calculated from the fitted value of K_a. [e] The binding constant for the complex formed between **TTF** and CBPQT[4+], previously measured in MeCN by the ^{1}H NMR single-point method, was determined (66, 67) to be 8,000 M^{−1}, and was found (67) to be 10,000 M^{−1} by the UV/Vis dilution method. [f] The binding constant for the complex formed between **BPTTF** and **CBPQT**[4+], previously measured in Me$_2$CO by the UV/Vis dilution method, was determined (68) to be 12,000 M^{−1}. [g] The binding constant for the complex formed between **DNP-OH** and **CBPQT**[4+], previously measured in MeCN by the UV/Vis dilution method, was determined (69) to be 990 M^{−1}. [h] The binding constant for the complex formed between **DNP-DEG** and **CBPQT**[4+], previously measured in MeCN by the UV/Vis dilution method, was determined (69) to be 25,400 M^{−1}. [i] The given thermodynamic values for **RATTF**[4+] and **RBPTTF**[4+] were obtained by the variable temperature CV measurements. [j] The linear fit to $\Delta G°/T$ vs. $1/T$ for **RATTF**[4+] produced a low R^2 of 0.4 because the $\Delta G°$ for **RATTF**[4+] was reasonably insensitive to temperature changes and therefore the data obtained reflects the standard error from the CV measurements.

The enthalpic contribution $\Delta H°$ to the binding affinity K_a between **DNP-DEG** and the **CBPQT**[4+] host is similar (Table 2-1) to that for **TTF-DEG**, but it is almost double that for **BPTTF-DEG**. This larger difference between the enthalpy changes ($\Delta H°$) of the two complexes is also represented in the bistable rotaxanes by the enthalpy change ($\Delta H°$) associated with the affinity of the CBPQT[4+] ring for the two recognition units. Correspondingly, the bistable rotaxane **RBPTTF**[4+] (−7.2 to −6.6

kcal/mol) shows a much higher $\Delta H°$ than **RATTF**$^{4+}$ (−1.2 to −2.8 kcal/mol). The direct consequence of this large $\Delta H°$ difference between the complexes of the **CBPQT**$^{4+}$ host with **DNP-DEG** and **BPTTF-DEG** is that the MSCC/GSCC ratio for **RBPTTF**$^{4+}$ exhibits a strong temperature dependence such that the ratio changes from 0.73 at 262 K to 0.25 at 284 K. The impact of temperature on equilibrium constants, K and their associated population ratios, MSCC/GSCC, are related by the Eyring equation ($\Delta H°/ T − \Delta S° = −R \ln K$) such that it is the enthalpic contribution that determines the temperature sensitivity.

Moreover, this variable ratio should be detectable in all three environments. In the solution phase and polymer gels, the MSCC/GSCC ratio can be quantified directly through CV measurements. In the MSTJs, the temperature dependent MSCC/GSCC ratio should be reflected in a temperature-dependent switching amplitude. By contrast with **RBPTTF**$^{4+}$, the smaller $\Delta H°$ difference for the binding of the CBPQT^{4+} ring to the TTF and DNP units should favor a relatively temperature-independent MSCC/GSCC ratio in **RATTF**$^{4+}$, with the GSCC remaining the dominant co-conformation at all temperatures and in all environments, a situation which is indeed observed. Irrespective of these differences in the ground state thermodynamics, for both **RATTF**$^{4+}$ and **RBPTTF**$^{4+}$, the actual electrochemically-driven switching mechanism should be the same.

2.3 Kinetics and Thermodynamics of Switching in Solution and in Polymer Electrolytes

The Heath and Stoddart research groups have previously demonstrated that the first oxidation potentials of bistable rotaxanes can be utilized to quantify the MSCC/GSCC ratios in the solution phase (40), for monolayers assembled onto Au surfaces (41), and for polymer electrolyte gels (39). In this section, I report on a set of similar variable time and temperature cyclic voltammetry (VTTCV) measurements in solution and polymer environments to probe the thermodynamics of the MSCC/GSCC equilibrium ratios for **RATTF**$^{4+}$ and **RBPTTF**$^{4+}$. From these measurements, I can extract free energy differences ($\Delta G°$ from figure 2-1b) between the two co-conformations.

I also utilized VTTCV to quantify the kinetics ($\Delta G^{\ddagger}$ from figure 2-1b) associated with the recovery of the equilibrium MSCC/GSCC distribution for **RBPTTF**$^{4+}$ and **RATTF**$^{4+}$. The relaxation kinetics for [2]rotaxane **RATTF**$^{4+}$ and for related TTF-based rotaxanes, were thoroughly investigated previously (39-41), while the equivalent VTTCV measurements for **RBPTTF**$^{4+}$ are reported here.

The VTTCV measurements are carried out as follows: two CV cycles are collected in succession, starting with the system at equilibrium. This first CV cycle displays peaks that can be assigned to the resting state populations of the MSCC and

GSCC, since the first oxidation potential of the TTF (BPTTF) group is sensitive to whether or not it is encircled by the $CBPQT^{4+}$ ring. The second cycle, if collected quickly enough, records a shift in the equilibrium population towards the one dominated by the MSCC. This shift is reflected in an increase in the area of the peak assigned to the MSCC, in coincidence with a decrease in the area for the GSCC peak. By controlling the time between the first and second CV cycles, and the temperature of the experiment, the kinetic parameters associated with the recovery of the MSCC/GSCC equilibrium ratio can be quantified. The representative CV data for **RBPTTF**$^{4+}$ showing the enhanced MSCC peak in the second cycle and scan-rate dependence for maintaining the MSCC peak in the second cycle were presented in figure 2-4.
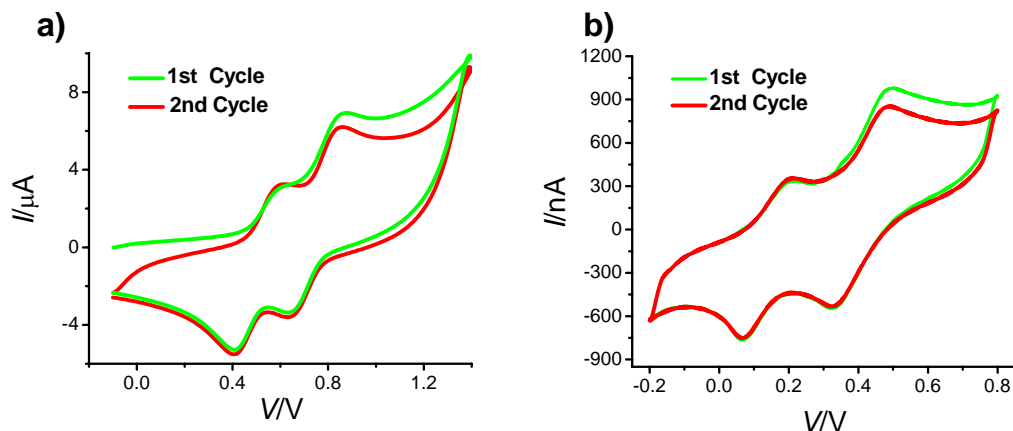
Figure 2-4. CV data of **RBPTTF**$^{4+}$ recorded in acetonitrile and polymer gel. Two cycles of CV data displayed enhanced MSCC peak in the second cycle in both (a) acetonitrile (measured at 800 mV/s, 262 K) and (b) polymer gel (measured at 130 mV/s, 303 K).

I first focus on utilizing VTTCV to probe the MSCC/GSCC population ratio at thermal equilibrium. The CVs of **RBPTTF**$^{4+}$ in the solution phase exhibit a peak at +530 mV, which corresponds to the BPTTF→BPTTF$^{\bullet+}$ oxidation of the proportion of the bistable rotaxane that exists in the MSCC (igure 2-4a). The smaller peak at +680 mV corresponds to the BPTTF→BPTTF$^{\bullet+}$ oxidation of the GSCC. The larger peak at +780 mV corresponds to the second oxidation (BPTTF$^{\bullet+}$→ BPTTF^{2+}). This second oxidation is independent of the co-conformation, since once the BPTTF$^{\bullet+}$ is formed, the CBPQT^{4+} ring moves to the DNP unit. The MSCC/GSCC population was thus measured as a function of temperature. For **RBPTTF**$^{4+}$, decreasing the temperature led to a significant increase in the MSCC/GSCC population ratio. The ratio, for

example, increases (figure 2-5a) more than two-fold (from around 0.3 to 0.7) as the temperature is decreased from 284 to 262 K. By comparison, for **RATTF**$^{4+}$, the MSCC/GSCC population ratio does not deviate significantly from 0.1, even when the rotaxane is probed (figure 2-5b) over a broader temperature range (248 – 283 K).
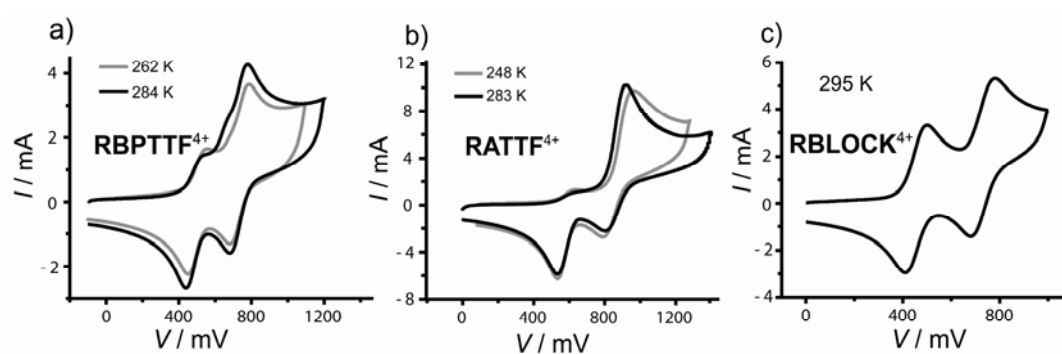
Figure 2-5. The first CV cycles of (a) **RBPTTF**$^{4+}$ recorded at 262 and 284 K, (b) **RATTF**$^{4+}$ recorded at 248 and 283 K and (c) **RBLOCK**$^{4+}$ recorded at 295 K (MeCN / 0.1 M TBAPF$_6$ / 200 mV s^{-1}). The peak assigned to the MSCC at ca. +500 mV for **RBPTTF**$^{4+}$ fluctuates more than for **RATTF**$^{4+}$ across different temperature ranges. The simple, dumbbell-like CV for **RBLOCK**$^{4+}$, displaying a full-intensity MSCC peak at ca. 500 mV, verifies that the CBPQT^{4+} ring is sterically blocked.

The relative temperature dependences of the MSCC/GSCC ratios for **RBPTTF**$^{4+}$ and for **RATTF**$^{4+}$ are consistent with the ITC investigations of the complexation of the **CBPQT**$^{4+}$ host with the individual **BPTTF-DEG**, **TTF-DEG**, and **DNP-DEG** guests that were discussed in the previous subchapter and presented in Table 2-1. Translating the behavior of the guests to what might be predicted for the

two bistable [2]rotaxanes, one expects that the enthalpic contribution $\Delta H° = (H°_{MSCC} - H°_{GSCC})$ should be significantly less than 0 for **RBPTTF**$^{4+}$. By comparison, the corresponding $\Delta H°$ for **RATTF**$^{4+}$ should be much closer to zero. As a consequence, the MSCC/GSCC ratio for **RBPTTF**$^{4+}$ varies more readily with temperature. The impact of temperature on equilibrium constants, K and their associated population ratios, MSCC/GSCC, are related by the Eyring equation ($\Delta H°/ T - \Delta S° = -R \ln K$) such that it is the enthalpic contribution that determines the temperature sensitivity.

Although it is not so straightforward to interpret, the long and flexible diethylene glycol chains appear to have an impact on the binding K_a and therefore the population ratios of the bistable rotaxanes. The DEG chains enhance (Table 2-1) the binding affinity for each of the three guests with the **CBPQT**$^{4+}$ host, but they do so by influencing the $\Delta H°$ and $\Delta S°$ of each component differently. For **TTF-DEG**, the DEG chains leads to better enthalpy but worse entropy. However, for the **DNP-DEG** and **BPTTF-DEG** guests, it is the opposite with the entropy contribution favoring binding and enthalpy disfavoring it, albeit only mildly so. Furthermore, it is known that when these DEG chains are attached to DNP and TTF units they are capable of wrapping themselves around the CBPQT^{4+} ring in order to acquire stabilizing, noncovalent [C–H···O] interactions (63, 64). Consequently, the significant enhancement of the enthalpic contribution to the complexation between **TTF-DEG**

and the **CBQPT**[4+] host by the DEG chains brings its ΔH° to within a few kcal / mol

of the **DNP-DEG** guest, leading to a relatively temperature insensitive MSCC/GSCC

ratio for the rotaxane **RATTF**[4+]. However, the DEG chains have little effect on the

$\Delta H°$ contribution to complexation of the **DNP-DEG** and **BPTTF-DEG** guests by the

CBPQT[4+] host such that they maintain their large and significant differences in

enthalpy within the **RBPTTF**[4+], leading to the rotaxane's correspondingly large

sensitivity of the population ratios to temperature. The DEG chains are thus an

essential factor influencing the temperature sensitivities of the MSCC/GSCC

population ratios of these bistable rotaxanes. The observation from the

electrochemical studies in the solution phase and in the polymer matrix provide a

view of both **RATTF**[4+] and **RBPTTF**[4+] that is completely consistent with the ITC

measurements on the subunits of the rotaxanes. It is also consistent with the molecular

structure differences between these two switches.
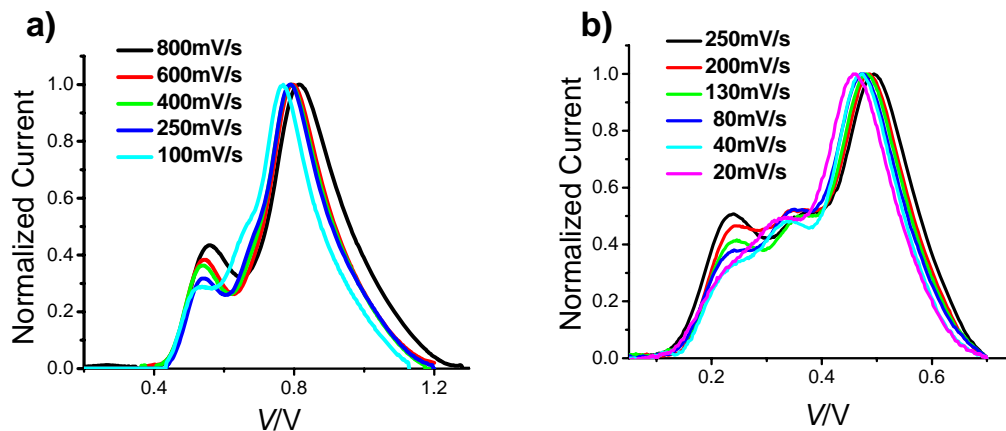
Figure 2-6. Normalized CV data in the second cycles. The larger MSCC peaks in the second cycle were maintained at faster scan rate in both (a) acetonitrile at 284 K and (b) polymer gel at 313 K. CV currents were normalized after subtracting base lines from original currents.

The relaxation kinetics and thermodynamics associated with the free energy barrier ($\Delta G^{\ddagger}$) for relaxation from the MSCC to the GSCC for **RATTF**$^{4+}$ and **RBPTTF**$^{4+}$ were also analyzed quantitatively. The viscosity of the acetonitrile solution phase and polymer gel were about 3.5 cp and 50,000 cp at 298 K, respectively. This large increase in viscosity is reflected in the slower first-order decay kinetics for **RBPTTF**$^{4+}$ as measured by VTTCV. Data for acetonitrile solution and the polymer gel are presented in figures 2-6 and 2-7. In addition to the viscosity effects, these plots also reveal how the thermally activated relaxation rates drop as the temperature is lowered.
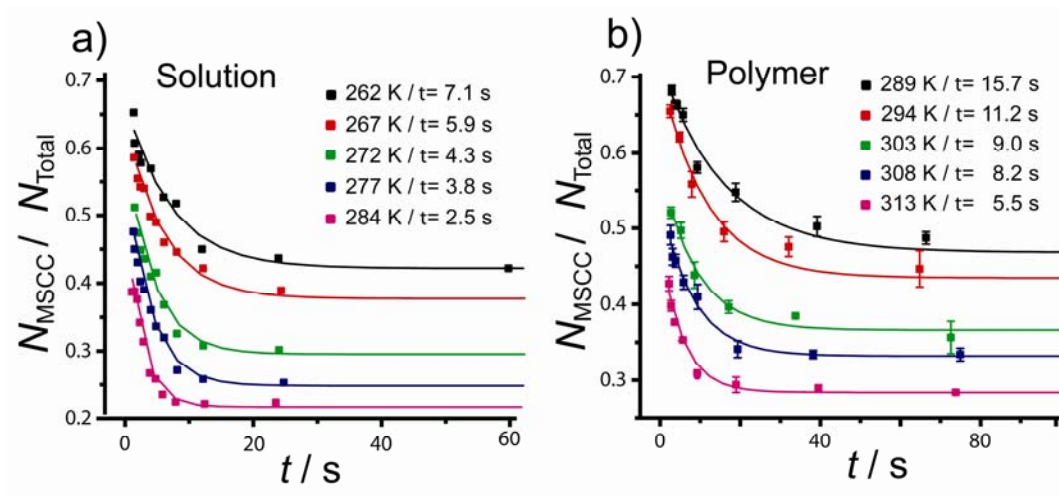
Figure 2-7. MSCC→equilbrium kinetics of **RBPTTF**$^{4+}$ in solution and polymer phases. Fitted exponential decay curves and time constants (t) obtained from the CV data for **RBPTTF**$^{4+}$ measured at various scan rates for each temperature in (a) solution and (b) polymer phases are presented.

It's instructive to notice that both the MSCC and GSCC are at significant concentrations under equilibrium conditions for **RBPTTF**$^{4+}$, especially at lower temperatures. The implication is that the reverse reaction GSCC → MSCC is occurring at a rate comparable to that of the forward reaction. In analyzing the relaxation kinetics, both processes should be taken into consideration. Thus, for the equilibrium reaction:

$$\text{MSCC} \underset{k_2}{\overset{k_1}{\rightleftharpoons}} \text{GSCC}$$
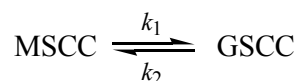
Eq. 1

the formula:

$$x_t = x_{eq} + (x_0 - x_{eq})\exp(-\frac{k_1}{1 - x_{eq}}t)$$

Eq. 2

is readily obtained, in which $x_t = \dfrac{N_{MSCC}}{N_{Total}}$ is the MSCC population ratio at time t,

$x_0 = x_{t=0}$, and $x_{eq} = x_{t\to\infty}$ is the MSCC population ratio at final equilibrium.

Experimental relaxation data were thus fitted with this formula to obtain the decay

time constant τ, and accordingly the rate constant for the forward reaction

$k_1 = \dfrac{1 - x_{eq}}{\tau}$. Note that when x_{eq} is small (i.e., for the case of **R(A)TTF⁴⁺**), the

formula naturally reduces to the more familiar formula for a simple first-order

reaction. $\Delta G^{\ddagger}$, $\Delta H^{\ddagger}$, $\Delta S^{\ddagger}$, and E_a are then fitted from the temperature dependence of

k_1. $G^{\ddagger}$ at each temperature was calculated from the Eyring equation:

$$\Delta G^{\neq} = -RT\ln\left(\frac{hk}{k_B T}\right)$$

where R, h, k and k_B are the gas constant, Planck's constant, the first-order rate

constant and Boltzmann constant, respectively. k corresponds to $(1 - x_{eq})/\tau$, where x_{eq}

is N_{MSCC}/N_{Total} at equilibrium and τ is 1/e decay time constant. $\Delta H^{\ddagger}$ and $\Delta S^{\ddagger}$ were

obtained from the regression analysis of Gibbs-Helmholtz plot, $\Delta G^{\ddagger}/T$ vs. $1/T$. The

activation barrier, E_a was calculated from the Arrhenius equation:

$$k = A\exp\left(\frac{-E_a}{RT}\right)$$

where A is the activation coefficient. E_a was obtained from a regression analysis of

the Arrhenius plots, ln k vs. 1/T. The kinetic data are summarized in Table 2-2

alongside values for **R(A)TTF**$^{4+}$. Note that the MSCC/GSCC population ratio for

RBPTTF^{4+}, as measured at long times (at equilibrium) shows (figure 2-7) significant

sensitivity to temperature, consistent with the thermodynamic descriptions and data

for the host-guest complexation. By contrast, **RATTF**$^{4+}$ displays only a small thermal

sensitivity in both the polymer and solution phase environments.

2.4 Kinetics and Thermodynamics of Molecular Switch Tunnel Junctions

The MSTJs investigated here contained a monolayer of the amphiphilic

bistable rotaxanes **RTTF**$^{4+}$ or **RBPTTF**$^{4+}$, or the sterically-blocked metastable-like

rotaxane **RBLOCK**$^{4+}$, sandwiched between an n-type poly-silicon bottom electrode

(passivated with the native oxide) and a metallic top electrode. The detailed

procedures relating to the fabrication and operation of these devices have been

reported (34-36). Briefly, the molecules are prepared as a Langmuir-Blodgett film and

then transferred as a compressed Langmuir monolayer (π = 30 mN/m) onto a substrate

pre-patterned with poly-silicon electrodes. A thin 10 nm Ti adhesion layer, followed

by a thicker 200 nm top Al layer is evaporated through a shadow mask using e-beam

evaporation to form the top electrodes. During this step, the substrate is held at room temperature at a source-sample distance of ~0.7 m. This procedure ensures that little or no substrate heating from the e-beam evaporation source occurs. The e-beam evaporation was processed at the deposition rate of $1 - 2$ Å/s under high vacuum (~5 x 10^{-7} Torr). For all experiments reported here, the bottom electrodes were 5 μm wide, n-type (doping level ~ 5 x 10^{-19} cm^{-3}) poly-Si, while the top electrodes were 10 μm wide. Each fabrication run produced approximately 100 MSTJ devices, and the results presented here were consistently observed in multiple devices across multiple fabrication runs, with temperature-dependent data collected in random sequence. More than 90 % of MSTJ devices showed the similar temperature-dependence reproducibly. The operational characteristics of MSTJs containing bistable catenanes and rotaxanes, but patterned at both larger and also much smaller dimensions, have been reported (36, 37).

CV measurements are not possible for MSTJs, but there are other electronic measurements that can be carried out to assess both the thermodynamic and kinetic properties of the bistable rotaxanes within the devices. The hypothesis – for both bistable catenanes and bistable rotaxanes – has been refined such that the MSCC represents the high-conducting, switch-closed state of the device, while the MSCC/GSCC ratio at equilibrium represents the low-conducting, switch-open state.

For an MSCC-dominated system, regardless of environment, reduction of the CBPQT^{4+} ring provides a rapid route towards recovering the equilibrium MSCC/GSCC distribution (35, 41). In the absence of such a reduction step, a device in the high-conductance state will relax to the equilibrium MSCC/GSCC ratio, according to a timescale described by $\Delta G^{\ddagger}$ (figure 2-1b). From a practical point of view (i.e., for memory devices), this relaxation process correlates to the volatility, or memory-retention characteristics, of the device. The volatility can be quantified by measuring the temperature dependence of the decay of the switch-closed, high conductance state of a device back to the switch-open state.

The equilibrium thermodynamic properties of the devices can also be inferred within MSTJs by considering that the high- and low-conductance states of the devices correlate with different MSCC/GSCC ratios. Thus, the temperature-dependent switching amplitude, normalized against the temperature-dependent transport characteristics of an MSTJ, opens a window into the thermodynamics of the molecules within the junction. Such a measurement provides a qualitative picture that can be compared against quantitative VTTCV measurements of the MSCC/GSCC ratios in other environments.
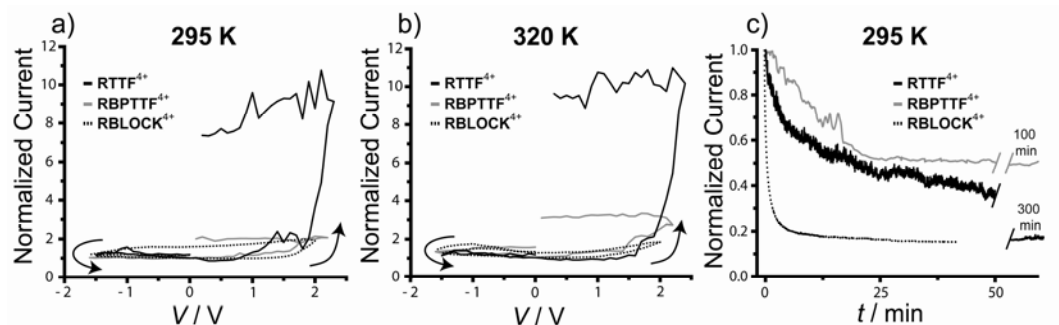
Figure 2-8. Switching responses of three rotaxanes within MSTJs. (a) and (b): Remnant molecular signature traces of the hysteretic switching responses. The arrows indicate the direction of the voltage sweep, and all currents were recorded at +0.1 V. The y-axis current was normalized by setting the initial (low-conductance state) current to 1. Note that the response of **RBPTTF**$^{4+}$ increases in amplitude at higher temperature, reflecting a decreasing MSCC/GSCC equilibrium ratio, while **RTTF**$^{4+}$ is relatively constant. There is a finite amount of field-induced polarization in **RBLOCK**$^{4+}$ that is almost undetectable at 320 K. (c) Relaxation of MSTJs from high-to-low conducting states recorded at 295 K. The characteristic relaxation times are: **RTTF**$^{4+}$ = 3450 s; **RBPTTF**$^{4+}$ = 660 s; **RBLOCK**$^{4+}$ = 60 s.

Measurements of the bistable character of MSTJs containing **RTTF**$^{4+}$, **RBTTF**$^{4+}$, and the **RBLOCK**$^{4+}$ control rotaxane are shown in figures 2-8a and 2-8b. This type of data is called a remnant molecular signature (34-36), and represents a nearly capacitance-free map of the hysteretic response of an MSTJ. Briefly, the x-axis of a remnant molecular signature plot correlates to a value of a voltage pulse that is applied across the junction. A train of voltage pulses, starting at 0 V and following the direction of the arrows shown on the plots, is applied to the MSTJ, and, after each

voltage pulse, the current through the MSTJ is monitored at +0.1 V. The remnant

molecular signature is a sequence of voltage pulses of 1 s that are applied to poly-Si

electrodes with 100 mV step sizes and, in between each pulse, is a read voltage of

+0.1 V held for 1.5 s to record the current. The metal top electrodes were connected to

ground through a preamplifier. The resulting normalized current is represented on the

y-axis. These hysteresis loops not only provide a key indicator that the MSTJs can be

switched reversibly between the high- and low-conducting states, but they also

qualitatively reflect the ground state MSCC/GSCC ratio, since the switching

amplitude is sensitive to this ratio. For the high-conductance state, in which the entire

population has been converted into the MSCC, the maximum current is controlled by

the intrinsic conductance properties of this co-conformation. However, for the low-

conductance state, the minimum conduction is not only controlled by the intrinsic

properties of the GSCC but also by the MSCC/GSCC ratio – a factor under

thermodynamic control. For instance, at 295 K **RBPTTF**$^{4+}$ and **RBLOCK**$^{4+}$ do not

appear to be 'good' switches, while the switching amplitude of **RTTF**$^{4+}$ is about a

factor of 8. At 320 K, the small hysteretic response for **RBLOCK**$^{4+}$ has further

diminished, but the hysteresis loop of **RBPTTF**$^{4+}$ has opened up to yield a switching

amplitude (i.e., the current measured in the high conductance state divided by the

current measured in the low conductance state) of over 3. This enhanced switching

amplitude presumably reflects a smaller MSCC/GSCC equilibrium ratio at the higher

temperature, and is consistent with what is observed for the solution and polymer

phase measurements for **RBPTTF**$^{4+}$. The switching amplitude of **RTTF**$^{4+}$ remains

fairly constant across this temperature range, consistent again with measurements in the

other environments. The MSCC $\rightarrow$ GSCC relaxation kinetics can be monitored by

measuring the time-dependence of the decay of the high-conductance to the low-

conductance state, and that data, for all three amphiphilic rotaxanes at 295 K, is

presented in figure 2-8c.
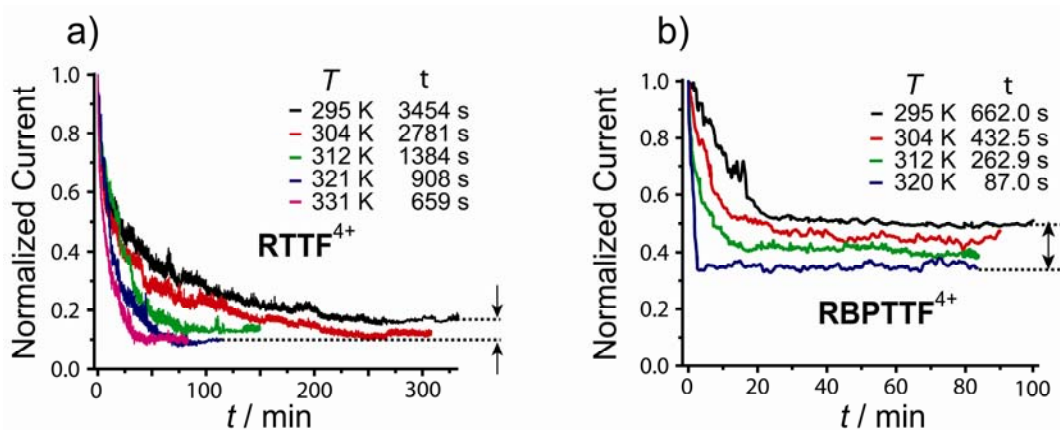
Figure 2-9. Decay curves of (a) **RTTF**$^{4+}$ and (b) **RBPTTF**$^{4+}$ MSTJs recorded as a
function of temperature. Note that the normalized switching amplitude of **RBPTTF**$^{4+}$
exhibits a strong temperature dependence.

The high- to low-conductance decay of all three rotaxanes exhibited different

temperature dependences. While MSTJs fabricated from **RBPTTF**$^{4+}$ and **RTTF**$^{4+}$

show strong temperature dependences – as the temperature was increased from 295 K

to 320 K, the 1/e decay time decreased by factors of 6 – 7 for those rotaxanes (figure 2-9) – **RBLOCK**$^{4+}$ exhibited a much weaker temperature dependence. MSTJs fabricated from **RBLOCK**$^{4+}$ were investigated over a broader temperature range (295 – 383 K) and the characteristic relaxation time decreased by only a factor of 2 or so over this entire range. This decay-rate data fitted well to a $1/T$ plot ($R^2 > 0.99$), which is at least consistent with existing models for dielectric relaxation (70), although measurements over an even broader temperature range would be required to establish this relationship more firmly. In any case, MSTJs fabricated from **RBLOCK**$^{4+}$ were poor switches at all temperatures investigated, and the small switching response that could be recorded exhibited a very different and much less-pronounced temperature-dependence, in comparison to MSTJs fabricated from **RBPTTF**$^{4+}$ and **RTTF**$^{4+}$. The switching amplitude can be recorded by either measuring the amplitude of the hysteresis loops from the remnant molecular signature data, or by measuring the time-dependent decay of the high- to the low-conductance state. Any molecular electronic junction for which charge transport is not strictly a quantum mechanical tunneling process will exhibit a strong temperature dependent conductance, i.e., charge transport is thermally activated, and the rate of transport increases with increasing temperature. This is the case for all three of the amphiphilic rotaxanes investigated here. However, this temperature-dependent component should depend only weakly upon molecular

structure – especially for molecules that are as similar as **RTTF**[4+], **RBPTTF**[4+], and

RBLOCK[4+], and should not be particularly sensitive to the MSCC/GSCC ratio within

a device. Thus, I remove this component of the temperature dependence by

normalizing the switching amplitude to the initial current value, measured at $t = 0$

after placing the switch into the high conductance state. The hypothesis is that the

(normalized) current at long times – i.e., when the system has reached equilibrium –

divided by the $t = 0$ current, should correlate qualitatively with the MSCC/GSCC ratio.

To the first order, the normalized current at equilibrium defined by the I_{OPEN}/I_{CLOSED}

ratio is approximately equal to N_{MSCC}/N_{Total} if the intrinsic conductance of the GSCC

is smaller by more than two orders of magnitude.

Based on the refined hypothesis that, the high-conductance (switch-closed)

state of an MSTJ corresponds to the MSCC but that the low-conductance (switch-

open) state is related to the MSCC/GSCC ratio at equilibrium, the measured current, I,

can be defined in terms of the intrinsic conductance properties of each co-

conformation and the percentage of the co-conformations N_{MSCC}/N_{Total} and

N_{GSCC}/N_{Total}.

Consequently, I_{OPEN} corresponds to a thermal equilibrium condition and is a

mixture of the GSCC and MSCC, whereas I_{CLOSED} is 100% of the MSCC. This model

influences the meaning of the ratio I_{OPEN}/I_{CLOSED}.

The conductance properties of these systems can be described as follows:

Firstly, the GSCC and MSCC have intrinsic current values I_{GSCC} and I_{MSCC}, which are constants at a certain temperature T. Therefore, at any time the current measured, I_t, is a summation of these two contributions. The magnitude of each contribution is scaled by the proportions of the GSCC (N_{GSCC}/N_{Total}) and MSCC (N_{MSCC}/N_{Total}) present in the mixture. This leads to the following general formula for the current I_t:

$$I_t = \left(\frac{N_{MSCC}}{N_{Total}}\right)_t * I_{MSCC} + \left(\frac{N_{GSCC}}{N_{Total}}\right)_t * I_{GSCC} \qquad \text{Eq. 3}$$

Therefore, for the trivial situation when I_{CLOSED} is measured at $t = 0$, I assume that $N_{GSCC} = 0$ and $N_{MSCC}/N_{Total} = 1$ confirming that $I_{CLOSED} = I_{MSCC}$ (see figure 2-10).
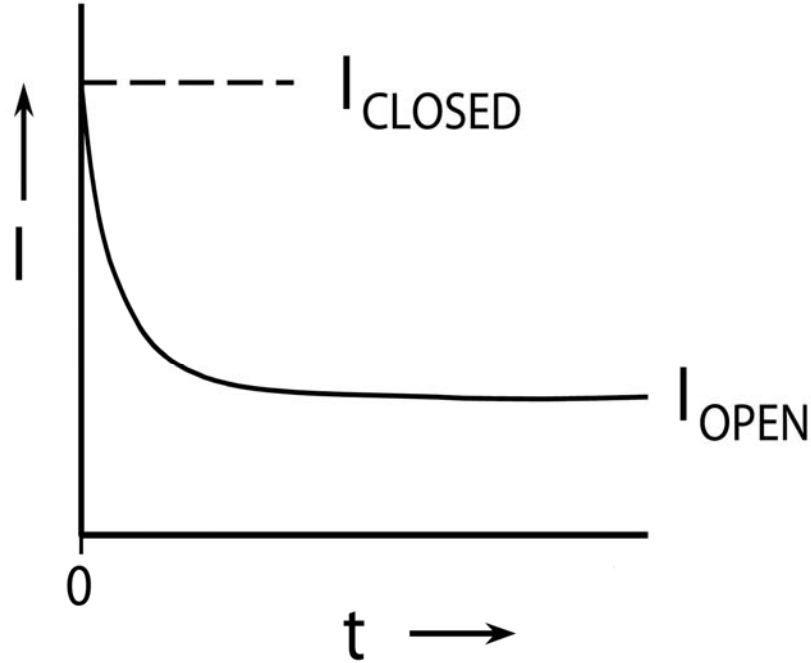
Figure 2-10. Schematic representation of a volatility curve defining I_{CLOSED} and I_{OPEN}.

Now consider what happens at thermal equilibrium ($t = \infty$), defined as I_{OPEN}:

$$I_{OPEN} = \left(\frac{N_{MSCC}}{N_{Total}}\right)_{\infty} * I_{CLOSED} + \left(\frac{N_{GSCC}}{N_{Total}}\right)_{\infty} * I_{GSCC} \qquad \text{Eq. 4}$$

Consequently, the ratio I_{OPEN}/I_{CLOSED}, which happens to be the inverse of the switching amplitude, can be expressed as:

$$\frac{I_{OPEN}}{I_{CLOSED}} = \left(\frac{N_{MSCC}}{N_{Total}}\right)_{\infty} + \left(\frac{N_{GSCC}}{N_{Total}}\right)_{\infty} * \frac{I_{GSCC}}{I_{CLOSED}} \qquad \text{Eq. 5}$$

If the intrinsic conductance of the GSCC is very small compared to I_{CLOSED}, the term

I_{GSCC}/I_{CLOSED} goes to zero and therefore:

$$I_{OPEN}/I_{CLOSED} = N_{MSCC}/N_{Total} \qquad \text{Eq. 6}$$

For example, in the case of **R(A)TTF^{4+}**, $N_{MSCC}/N_{Total} = 1/10$ and assuming an intrinsic

conductance of the GSCC that is 100 times smaller than the MSCC, $I_{GSCC}/I_{Closed} =$ 1/100 then the ratio at $t = \infty$ becomes:

$$I_{OPEN}/I_{CLOSED} = 1/10 + (9/10*1/100) = 1/10 + 9/1000 = 0.1 + 0.009 = 0.109$$

Consider also how **RBPTTF**[4+] behaves at low temperatures (MSCC/GSCC = 3:4):

$$I_{OPEN}/I_{CLOSED} = 3/7 + (4/7*1/100) = 0.43 + 0.006 = 0.436$$

In other words, the ratio of N_{MSCC}/N_{Total} dominates the I_{OPEN}/I_{CLOSED} measured ratio at equilibrium and therefore the switching amplitude in the condition when the intrinsic conductance of the GSCC is small.

Whereas in the condition when the intrinsic conductance of the GSCC were higher such as if $I_{GSCC}/I_{CLOSED} = 1/10$, then for **R(A)TTF**[4+]:

$$I_{OPEN}/I_{CLOSED} = 1/10 + (9/10*1/10) = 1/10 + 9/100 = 0.1 + 0.09 = 0.19$$

and for **RBPTTF**[4+]:

$$I_{OPEN}/I_{CLOSED} = 3/7 + (4/7*1/10) = 0.43 + 0.06 = 0.49$$

Comparing between the two cases, where I_{GSCC} is comparatively smaller (1%) or larger (10%) leads to switching amplitudes for **R(A)TTF**[4+] of 9 and 5, respectively, whereas for **RBPTTF**[4+] they correspond to 2.3 and 2.0.

Small relative intrinsic conductances of the GSCC compared to the MSCC are not so unlikely and have been calculated (61, 62) for related TTF-containing bistable catenanes, based on the theory of coherent electron transport, to be approximately

1/10,000.

In figure 2-9, I present such normalized decay curves, for various temperatures, for both **RTTF**[4+] and **RBPTTF**[4+]. Note two things about the data of figure 2-9. First, the curves clearly represent activated processes, since, for both bistable rotaxanes, the relaxation times decrease rapidly with increasing temperature. Second, the switching amplitude for **RTTF**[4+] is relatively temperature independent, exhibiting almost an order-of-magnitude difference in the (normalized) current change between the high- and low-conductance states for all temperatures. By contrast, the switching amplitude for **RBPTTF**[4+] exhibits a strong temperature dependence over the same range. This observation is consistent with the remnant molecular signature data presented in figure 2-8. Also, it is consistent with the behavior of the corresponding bistable rotaxanes (**RATTF**[4+] and **RBPTTF**[4+]) in the other environments, as well as the ITC data obtained from host-guest complexation experiments.

2.5 A Summary of Kinetic and Thermodynamic Studies in All of Three Environments

The temperature-dependent thermodynamic and relaxation kinetic data for all environments are presented in figures 2-11a and 2-11b, respectively. In figure 2-11a I have plotted the temperature-dependent ratios as N_{MSCC}/N_{TOTAL}, quantitatively

measured in the solution-phase and polymer environments. For the MSTJs, this ratio cannot be quantified, but the temperature-dependent switching amplitude I_{OPEN}/I_{CLOSED} provides for qualitative comparison with the other environments. For the relaxation kinetics, data for the two TTF-containing rotaxanes (**R(A)TTF**$^{4+}$) and **RBPTTF**$^{4+}$ are plotted in the form of Eyring plots, in order to quantify (Table 2-2) $\Delta G^{\ddagger}$, $\Delta H^{\ddagger}$, and $\Delta S^{\ddagger}$ in all three environments.

Table 2-2. Kinetics data for the relaxation from the MSCC to the GSCC for **RBPTTF**[4+] and the free energy barriers for **RATTF**[4+] and **RTTF**[4+]. Data for solution, polymer and MSTJ were obtained from variable temperature CVs and from measurements of the relaxation of a MSTJ from the high to the low conductance state.

| Environ. | τ_{298} | k_{298} | $\Delta G^{\ddagger}_{298}$ | $\Delta H^{\ddagger}$ | $\Delta S^{\ddagger}$ | E_a | $\Delta G^{\ddagger}_{298}$ | $\Delta G^{\ddagger}_{298}$ |
	[s]	[s^{-1}]	[kcal·mol^{-1}]	[kcal·mol^{-1}]	[cal·$mol^{-1}K^{-1}$]	[kcal·mol^{-1}]	**RATTF**[4+]	**RTTF**[4+]
Solution[a]	1.26 ± 0.10	0.69 ± 0.05	17.69 ± 0.05	8.4 ± 0.5	-31.0 ± 1.7	9.0 ± 0.5	16.2 ± 0.3	–
Polymer[b]	10.2 ± 0.12	0.059 ± 0.001	19.15 ± 0.01	8.4 ± 1.1	-36.0 ± 3.4	9.0 ± 1.0	18.1 ± 0.2	–
MSTJ	624 ± 82	$(8.4 \pm 0.8) \times 10^{-4}$	21.7 ± 0.1	16.1 ± 1.4	-18.7 ± 4.1	16.7 ± 1.3	–	22.21 ± 0.04

[a] Solution-phase data was obtained for 1 mM samples dissolved in MeCN (0.1 M TBAPF$_6$) using a glassy carbon working electrode. All potentials were referenced to a Ag/AgCl reference electrode (40). [b] Polymer-phase data was obtained in a polymer matrix - w:w:w:w ratios of 70:7:20:3 for MeCN:polymethylmethacrylate:propylene carbonate:LiClO$_4$. The sample was spread onto three lithographically-patterned Pt electrodes (50 nm) on top of Ti (10 nm) (working, counter, reference)(39). The $\Delta H^{\ddagger}$ and $\Delta S^{\ddagger}$ were obtained from an average of many devices while the Eyring plot in figure 2-10 b represents just one device.
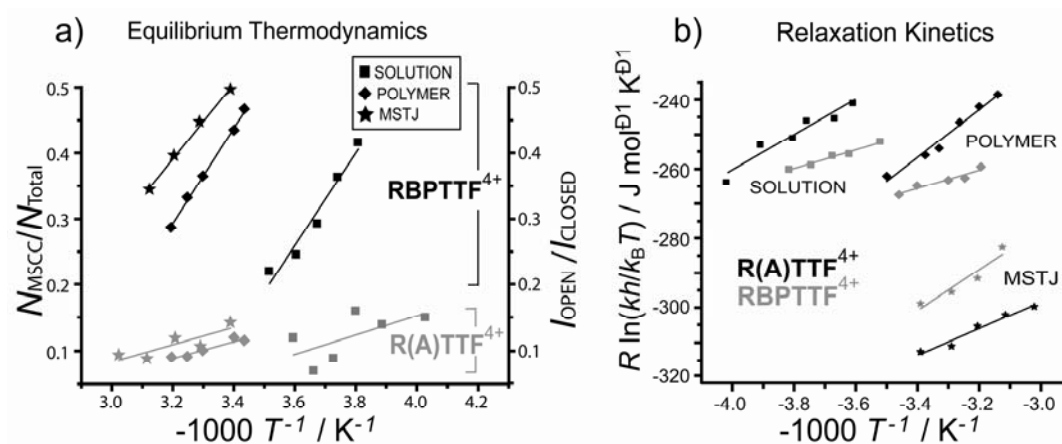
Figure 2-11. (a) The temperature-dependent GSCC/MSCC equilibria for all three environments are presented. Solution and polymer phase data (N_{MSCC}/N_{Total}) were recorded for **RATTF^{4+}** and **RBPTTF^{4+}** and are based upon quantitative electrochemical measurements of the MSCC/GSCC ratios. The MSTJ data, which were recorded for **RTTF^{4+}** and **RBPTTF^{4+}**, show the temperature-dependent switching amplitude (I_{OPEN}/I_{CLOSED}), and represent a qualitative measurement of the N_{MSCC}/N_{Total} ratio, based upon the proposed switching mechanism. Note that the large (enthalpically driven) temperature dependence for **RBPTTF^{4+}**, and the relative temperature independence of **RATTF^{4+}** and **RTTF^{4+}** (**R(A)TTF^{4+}**) is reflected in all environments. (b) Eyring plots of the MSCC $\rightarrow$ GSCC (or high-conducting MSTJ $\rightarrow$ low-conducting MSTJ) relaxation process, for all three environments.

I first consider the kinetic data of figure 2-11b and Table 2-2. For the case of **RBPTTF^{4+}**, the free energy barrier ($\Delta G^{\ddagger}$) to relaxation at 298 K increases from 17.7 to 19.2 to 21.7 kcal/mol upon moving from acetonitrile solution to polymer gels to MSTJs. For **R(A)TTF^{4+}**, the situation is qualitatively similar. Both rotaxanes exhibit an increase in the energy barrier ($\Delta G^{\ddagger}$) from the solution to polymer phase by between

1 and 2 kcal/mol. However, the $\Delta G^{\ddagger}$ increase in moving from the polymer to the MSTJ is significantly larger for **R(A)TTF**$^{4+}$ than for **RBPTTF**$^{4+}$ (2.5 vs. 4.1 kcal/mol). This difference may be related to the differences in packing between the Langmuir monolayers of the amphiphilic rotaxanes. Both monolayers were transferred onto the electrode-patterned substrate at a pressure of 30 mN/m. However, the **RTTF**$^{4+}$ rotaxanes occupy 92 ± 3 Å^2/molecule, while the **RBPTTF**$^{4+}$ rotaxanes occupy 122 ± 5 Å^2/molecule. Thus, the packing of **RBPTTF**$^{4+}$ is influenced by a combination of the high MSCC/GSCC ratio and the bulkier hydrophilic stopper. These differences lead to a 30% increase in the area/molecule over a similarly compressed film of **RTTF**$^{4+}$. Nevertheless, for both amphiphilic, bistable rotaxanes, the data in figures 2-8 and 2-9 indicate a qualitatively similar switching mechanism, regardless of physical environment.

The thermodynamic data of figure 2-10a are apparently more reflective of the structural differences between **R(A)TTF**$^{4+}$ and **RBPTTF**$^{4+}$, rather than the physical environment of these molecules. In all environments, **RBPTTF**$^{4+}$ exhibits a strongly temperature-dependent switching amplitude that can be related back to the temperature-dependence of the MSCC/GSCC ratio. In turn, this behavior can be connected to the free energy difference between the two host-guest complexes, **BPTTF-DEG⊂CBPQT**$^{4+}$ and **DNP-DEG⊂CBPQT**$^{4+}$, and the fact that the enthalpic

contribution to the free energy is very different for these two complexes. The temperature dependence of the MSCC/GSCC ratio of **RBPTTF**$^{4+}$ is slightly more pronounced for the solution and polymer environments than for the MSTJ. This is likely due to the fact that the MSTJ constitutes a more sterically crowded environment. Nevertheless, the degree to which the free energy landscape of the bistable **RBPTTF**$^{4+}$ is reflected in the properties of this molecule, regardless of environment, is striking.

In a similar way, the temperature independent switching of **R(A)TTF**$^{4+}$ can also be rationalized within a self-consistent picture that connects across all environments as well as to the free energy differences between the **TTF-DEG⊂CBPQT**$^{4+}$ and **DNP-DEG⊂CBPQT**$^{4+}$ host-guest complexes. From the point of view of an MSTJ-based memory device, **RTTF**$^{4+}$ constitutes a much superior switch than does **RBPTTF**$^{4+}$. First, it exhibits a stable switching amplitude over a reasonably broad temperature range. Second, an **RTTF**$^{4+}$-based MSTJ remains in the high-conducting (MSCC-dominated) state 5 times longer than an **RBPTTF**$^{4+}$-based MSTJ at 295 K, and 10 times longer at 320 K, implying a less volatile (and more useful) switch.

2.6 Conclusion

I have investigated two classes of bistable rotaxanes – one containing a TTF unit and the other a BPTTF unit – across different environments. Quantifying the relaxation rates in one critical step of the switching cycle enables us, not only to validate the proposed switching mechanism and its universality, but also to correlate switching kinetic rates with the nature of the environment. The trend in the kinetics and the validity of the switching mechanism are consistent and similar for both classes of bistable rotaxanes. Nevertheless, temperature-dependent thermodynamic measurements can reflect subtle differences between the various switching molecules. By replacing the TTF unit in the bistable rotaxanes with a BPTTF unit, the equilibrium MSCC/GSCC population ratio, which influences the low-conductance state in MSTJs, and the temperature sensitivity of this ratio, was altered considerably. Correspondingly, the switching amplitude between the high-conductance state and the now thermally-sensitive low-conductance state, changes significantly with temperature. Binding constant measurements for the complexation of model guests with the **CBPQT**$^{4+}$ host verify that the population ratio and its temperature sensitivity are likely related to the different binding strengths of the DEG-disubstituted TTF and BPTTF units. Enthalpy is found to play a crucial role in determining these binding strengths. To summarize these results, it is evident that the kinetics rates of the

molecular mechanical switching process are strongly influenced by both environment and molecular structure, while the thermodynamics values that describe the bistable nature of these molecular switches are relatively independent of environment, but strongly dependent upon molecular structure. This realization represents a key element in the emerging paradigm of molecular electronics.

2.7 References

1.   Heath, J. R. & Ratner, M. A. (2003) *Physics Today* 56, 43-49.

2.   McCreery, R. L. (2004) *Chem. Mater.* 16, 4477-4496

3.   Nitzan, A. (2001) *Ann. Rev. Phys. Chem.* 52, 681-750.

4.   Allara, D. L., Dunbar, T. D., Weiss, P. S., Bumm, L. A., Cygan, M. T., Tour, J. M., Reinerth, W. A., Yao, Y., Kozaki, M. & Jones, L. (1998) in *Molecular Electronics: Science and Technology*, Vol. 852, pp. 349-370.

5.   Chen, J., Reed, M. A., Rawlett, A. M. & Tour, J. M. (1999) *Science* 286, 1550-1552.

6.   Chen, Y., Jung, G. Y., Ohlberg, D. A. A., Li, X. M., Stewart, D. R., Jeppesen, J. O., Nielsen, K. A., Stoddart, J. F. & Williams, R. S. (2003) *Nanotechnology* 14, 462-468.

7.   Donhauser, Z. J., Mantooth, B. A., Kelly, K. F., Bumm, L. A., Monnell, J. D.,

Stapleton, J. J., Price, D. W., Rawlett, A. M., Allara, D. L., Tour, J. M. & Weiss, P. S. (2001) *Science* 292, 2303-2307.

8. Dunbar, T. D., Cygan, M. T., Bumm, L. A., McCarty, G. S., Burgin, T. P., Reinerth, W. A., Jones, L., Jackiw, J. J., Tour, J. M., Weiss, P. S. & Allara, D. L. (2000) *J. Phys. Chem. B* 104, 4880-4893.

9. Kornilovitch, P. E., Bratkovsky, A. M. & Williams, R. S. (2002) *Phys. Rev. B* 66, 165436.

10. Lee, I. C. & Frank, C. W. (2004) *Langmuir* 20, 5809-5828.

11. McConnell, H. (1961) *J. Chem. Phys.* 35, 508-515.

12. Polymeropoulos, E. E. & Sagiv, J. (1978) *J. Chem. Phys.* 69, 1836-1847.

13. Richter, C. A., Stewart, D. R., Ohlberg, D. A. A. & Williams, R. S. (2005) *Appl. Phys. A - Mat. Sci. & Proc.* 80, 1355-1362.

14. Smalley, J. F., Sachs, S. B., Chidsey, C. E. D., Dudek, S. P., Sikes, H. D., Creager, S. E., Yu, C. J., Feldberg, S. W. & Newton, M. D. (2004) *J. Am. Chem. Soc.* 126, 14620-14630.

15. Vincett, P. S. & Roberts, G. G. (1980) *Thin Solid Films* 68, 135-171.

16. Aviram, A. & Ratner, M. A. (1974) *Chem. Phys. Lett.* 29, 277-283.

17. Ashwell, G. J. & Gandolfo, D. S. (2001) *J. Mat. Chem.* 11, 246-248.

18. Ashwell, G. J., Gandolfo, D. S. & Hamilton, R. (2002) *J. Mat. Chem.* 12, 416-

420.

19.   Ashwell, G. J., Gandolfo, D. S. & Hamilton, R. (2002) *J. Mat. Chem.* 12, 416-

        420.

20.   Ashwell, G. J., Sambles, J. R., Martin, A. S., Parker, W. G. & Szablewski, M.

        (1990) *J. Chem.Soc.-Chem. Comm.* 1374-1376.

21.   Ashwell, G. J., Tyrrell, W. D. & Whittam, A. J. (2004) *J. Am. Chem. Soc.* 126,

        7102-7110.

22.   Chang, S. C., Li, Z. Y., Lau, C. N., Larade, B. & Williams, R. S. (2003) *Appl.*

        Phys. Lett. 83, 3198-3200.

23.   Ho, G., Heath, J. R., Kondratenko, M., Perepichka, D. F., Arseneault, K.,

        Pezolet, M. & Bryce, M. R. (2005) *Chem. Eur. J.* 11, 2914-2922.

24.   Krebs, F. C., Spanggaard, H., Rozlosnik, N., Larsen, N. B. & Jorgensen, M.

        (2003) *Langmuir* 19, 7873-7880.

25.   Lau, C. N., Stewart, D. R., Williams, R. S. & Bockrath, M. (2004) *Nano Lett.*

        4, 569-572.

26.   Maruccio, G., Cingolani, R. & Rinaldi, R. (2004) *J. Mat. Chem.* 14, 542-554.

27.   Metzger, R. M. (1999) *Acc. Chem. Res.* 32, 950-957.

28.   Metzger, R. M. (2003) *Chem. Rev.* 103, 3803-3834.

29.   Metzger, R. M., Chen, B., Hopfner, U., Lakshmikantham, M. V., Vuillaume,

D., Kawai, T., Wu, X. L., Tachibana, H., Hughes, T. V., Sakurai, H., Baldwin, J. W., Hosch, C., Cava, M. P., Brehmer, L. & Ashwell, G. J. (1997) *J. Am. Chem. Soc.* 119, 10455-10466.

30. Metzger, R. M., Xu, T. & Peterson, I. R. (2001) *J. Phys. Chem. B* 105, 7280-7290.

31. Ng, M. K. & Yu, L. P. (2002) *Angew. Chem. Int. Ed.* 41, 3598-3601.

32. Stewart, D. R., Ohlberg, D. A. A., Beck, P. A., Chen, Y., Williams, R. S., Jeppesen, J. O., Nielsen, K. A. & Stoddart, J. F. (2004) *Nano Lett.* 4, 133-136.

33. Shipway, A. N. & Willner, I. (2001) *Acc. Chem. Res.* 34, 421-432.

34. Collier, C. P., Jeppesen, J. O., Luo, Y., Perkins, J., Wong, E. W., Heath, J. R. & Stoddart, J. F. (2001) *J. Am. Chem. Soc.* 123, 12632-12641.

35. Collier, C. P., Mattersteig, G., Wong, E. W., Luo, Y., Beverly, K., Sampaio, J., Raymo, F. M., Stoddart, J. F. & Heath, J. R. (2000) *Science* 289, 1172-1175.

36. Luo, Y., Collier, C. P., Jeppesen, J. O., Nielsen, K. A., DeIonno, E., Ho, G., Perkins, J., Tseng, H. R., Yamamoto, T., Stoddart, J. F. & Heath, J. R. (2002) *Chemphyschem* 3, 519-525.

37. Diehl, M. R., Steuerman, D. W., Tseng, H. R., Vignon, S. A., Star, A., Celestre, P. C., Stoddart, J. F. & Heath, J. R. (2003) *Chemphyschem* 4, 1335-1339.

38. Yu, H. B., Luo, Y., Beverly, K., Stoddart, J. F., Tseng, H. R. & Heath, J. R.

(2003) *Angew. Chem. Int. Ed.* 42, 5706-5711.

39.   Steuerman, D. W., Tseng, H. R., Peters, A. J., Flood, A. H., Jeppesen, J. O., Nielsen, K. A., Stoddart, J. F. & Heath, J. R. (2004) *Angew. Chem. Int. Ed.* 43, 6486-6491.

40.   Flood, A. H., Peters, A. J., Vignon, S. A., Steuerman, D. W., Tseng, H. R., Kang, S., Heath, J. R. & Stoddart, J. F. (2004) *Chem. Eur. J.* 10, 6558-6564.

41.   Tseng, H. R., Wu, D. M., Fang, N. X. L., Zhang, X. & Stoddart, J. F. (2004) *Chemphyschem* 5, 111-116.

42.   Jeppesen, J. O., Nielsen, K. A., Perkins, J., Vignon, S. A., Di Fabio, A., Ballardini, R., Gandolfi, M. T., Venturi, M., Balzani, V., Becher, J. & Stoddart, J. F. (2003) *Chem. Eur. J.* 9, 2982-3007.

43.   Jeppesen, J. O., Perkins, J., Becher, J. & Stoddart, J. F. (2001) *Angew. Chem. Int. Ed.* 40, 1216-1221.

44.   Jeppesen, J. O., Takimiya, K., Jensen, F., Brimert, T., Nielsen, K., Thorup, N. & Becher, J. (2000) *J. Org. Chem.* 65, 5794-5805.

45.   Kang, S. S., Vignon, S. A., Tseng, H. R. & Stoddart, J. F. (2004) *Chem. Eur. J.* 10, 2555-2564.

46.   Tseng, H. R., Vignon, S. A., Celestre, P. C., Perkins, J., Jeppesen, J. O., Di Fabio, A., Ballardini, R., Gandolfi, M. T., Venturi, M., Balzani, V. & Stoddart,

J. F. (2004) *Chem. Eur. J.* 10, 155-172.

47.   Yamamoto, T., Tseng, H. R., Stoddart, J. F., Balzani, V., Credi, A., Marchioni, F. & Venturi, M. (2003) *Col. Czech. Chem. Comm.* 68, 1488-1514.

48.   Katz, E., Lioubashevsky, O. & Willner, I. (2004) *J. Am. Chem. Soc.* 126, 15520-15532.

49.   Long, B., Nikitin, K. & Fitzmaurice, D. (2003) *J. Am. Chem. Soc.* 125, 15490-15498.

50.   Ryan, D., Rao, S. N., Rensmo, H., Fitzmaurice, D., Preece, J. A., Wenger, S., Stoddart, J. F. & Zaccheroni, N. (2000) *J. Am. Chem. Soc.* 122, 6252-6257.

51.   Alteri, A., Gatti, F. G., Kay, E. R., Leigh, D. A., Martel, D., Paolucci, F., Slawin, A. M. Z. & Wong, J. K. Y. (2003) *J. Am. Chem. Soc.* 125, 8644-8654.

52.   Altieri, A., Bottari, G., Dehez, F., Leigh, D. A., Wong, J. K. Y. & Zerbetto, F. (2003) *Angew. Chem. Int. Ed.* 42, 2296-2300.

53.   Brouwer, A. M., Frochot, C., Gatti, F. G., Leigh, D. A., Mottier, L., Paolucci, F., Roffia, S. & Wurpel, G. W. H. (2001) *Science* 291, 2124-2128.

54.   Cecchet, F., Rudolf, P., Rapino, S., Margotti, M., Paolucci, F., Baggerman, J., Brouwer, A. M., Kay, E. R., Wong, J. K. Y. & Leigh, D. A. (2004) *J.Phys.Chem. B* 108, 15192-15199.

55.   Collin, J. P., Gavina, P. & Sauvage, J. P. (1997) *New J. Chem.* 21, 525-528.

56.   Livoreil, A., Dietrichbuchecker, C. O. & Sauvage, J. P. (1994) *J. Am. Chem. Soc.* 116, 9399-9400.

57.   Poleschak, I., Kern, J. M. & Sauvage, J. P. (2004) *Chem. Comm.*, 474-476.

58.   Raehm, L., Kern, J. M. & Sauvage, J. P. (1999) *Chem. Eur. J.* 5, 3310-3317.

59.   Norgaard, K., Jeppesen, J. O., Laursen, B. A., Simonsen, J. B., Weygand, M. J., Kjaer, K., Stoddart, J. F. & Bjornholm, T. (2005) *J. Phys. Chem. B* 109, 1063-1066.

60.   Laursen, B. W., Nygaard, S., Jeppesen, J. O. & Stoddart, J. F. (2004) *Org. Lett.* 6, 4167-4170.

61.   Deng, W. Q., Muller, R. P. & Goddard, W. A. (2004) *J. Am. Chem. Soc.* 126, 13562-13563.

62.   Kim, Y. H., Jang, S. S., Jang, Y. H. & Goddard, W. A. (2005) *Phys. Rev. Lett.* 94, 156801.

63.   Houk, K. N., Menzer, S., Newton, S. P., Raymo, F. M., Stoddart, J. F. & Williams, D. J. (1999) *J. Am. Chem. Soc.* 121, 1479-1487.

64.   Raymo, F. M., Bartberger, M. D., Houk, K. N. & Stoddart, J. F. (2001) *J. Am. Chem. Soc.* 123, 9264-9267.

65.   Blandamer, M. J., Cullis, P. M. & Engberts, J. (1998) *J. Chem. Soc. - Far. Trans.* 94, 2261-2267.

66.   Ashton, P. R., Ballardini, R., Balzani, V., Boyd, S. E., Credi, A., Gandolfi, M. T., GomezLopez, M., Iqbal, S., Philp, D., Preece, J. A., Prodi, L., Ricketts, H. G., Stoddart, J. F., Tolley, M. S., Venturi, M., White, A. J. P. & Williams, D. J. (1997) *Chem. Eur. J.* 3, 152-170.

67.   Ashton, P. R., Balzani, V., Becher, J., Credi, A., Fyfe, M. C. T., Mattersteig, G., Menzer, S., Nielsen, M. B., Raymo, F. M., Stoddart, J. F., Venturi, M. & Williams, D. J. (1999) *J. Am. Chem. Soc.* 121, 3951-3957.

68.   Nielsen, M. B., Jeppesen, J. O., Lau, J., Lomholt, C., Damgaard, D., Jacobsen, J. P., Becher, J. & Stoddart, J. F. (2001) *J. Org. Chem.* 66, 3559-3563.

69.   Castro, R., Nixon, K. R., Evanseck, J. D. & Kaifer, A. E. (1996) *J. Org. Chem.* 61, 7298-7303.

70.   Iwamoto, M. & Wu, C. X. (1997) *Phys. Rev. E* 56, 3721-3724.